Sensitive response of GNP/epoxy coatings as strain sensors: analysis of tensile-compressive and reversible cyclic behavior.

Xoan F. Sánchez-Romate[1], R. Moriche[*1,2], A. Jiménez-Suárez[1], M. Sánchez[1], S. G. Prolongo[1], A. Ureña[1]

[1]Materials Science and Engineering Area, University Rey Juan Carlos, C/Tulipán s/n, Móstoles, 28933, Madrid, Spain
[2]Dpto. de Física de la Materia Condensada, ICMS, CSIC-Universidad de Sevilla, Apdo. 1065, 41080 Sevilla, Spain

*Corresponding author: rmoriche@us.es

Abstract

The electromechanical performance and reversibility of sensitive GNP/epoxy strain sensors were experimentally and theoretically analyzed. Under tensile loads, the strain sensors showed lower sensitivity and more linearity than bulk sensors, behavior attributed to a slight preferential orientation of the GNPs along the in-plane direction. The Gauge Factor (GF) obtained was 9.1 ± 0.9 and 11 ± 1 for strain values up to 0.005 mm/mm and above 0.015 mm/mm, respectively. In contrast, the electromechanical response when subjected to compressive strain is more complex and three different regions are distinguished: (I) diminution, (II) stabilization and (III) increase of the normalized electrical resistance. Here, GF under compressive loads was negative at low strain values (region I), being -13 ± 2, and positive at high strain (region III), with a value of 8 ± 1. Theoretical analysis revealed that at low strain, there is prevalence of in-plane tunneling mechanisms whereas at higher strain, the out of plane mechanisms dominate, explaining the apparently anomalous behavior at compressive loads. Additionally, strain sensors showed high reversibility with cyclic load in the electromechanical response, but under compressive forces, the loading-unloading electrical resistance curve was asymmetric due to the opening and closing of microcavities and defects in the vicinities of the GNPs.

Keywords: Polymer-matrix composites (PMCs), Graphene nanoplatelets, Electrical properties, Analytical modelling, Sensors, SHM

1. Introduction

Carbon nanoparticles show exceptional properties as it has been observed in many studies, leading to Young's Modulus of 250 GPa to 1 TPa as well as superior thermal and electrical conductivities, ~ 3000 W/mK and ~ 10^6 S/m, respectively [1-4]. In fact, they enhance electrical conductivity of typical non-conductive polymers making them electrically conductive by the creation of percolating networks inside the material, leading to electrical conductivities up to 1000-1500 S/cm [5-9]. For these reasons, their use has increased during the last years, covering a wide range of applications such as lightning strike protection, electromagnetic shielding or structural health monitoring (SHM) [10-12]. Specifically, their use for SHM purposes is particularly interesting as these percolating networks change when subjected to applied strain, promoting a variation of the electrical resistance that can be monitored [13-15]. More specifically, they have demonstrated excellent capabilities for real-time curing behavior monitoring purposes [16].

To date, there are many research on sensing capabilities of graphene nanoplatelets (GNPs), proving their exceptional potential for SHM applications. In this regard, many studies have demonstrated their high electrical sensitivity when subjected to mechanical strain. In fact, the gauge factor (GF), defined as the change in normalized resistance divided by the applied strain, is much higher than carbon nanotube (CNT) based nanocomposites [17-19]. This is due to the combined effect of their piezoresistive behavior as well as the tunneling mechanisms between adjacent carbon nanoparticles, which are more prevalent in case of GNPs due to their 2D structure [20,21]. Therefore, their use as strain gauges is attracting the interest of many researchers since their addition induces a drastic improvement on mechanical performance and yields to high gauge factors (from 2 at low strain levels up to around 150 for flexible sensors) [9,15,22].

This work, thus, aims to explore the strain sensing capabilities of GNP based composites in their application as strain surface sensors. Here, dispersion technique plays a crucial role in the behavior of the strain sensors. In this context, ultrasonication process seems to be a powerful dispersion technique to achieve a good homogenization of GNPs inside the non-conductive media

[9,22]. However, three roll milling process has proven to be a complementary technique as it induces some stretching effects on nanoplatelets that improves the dispersion state of the nanofillers [23]. For this reason, a combined ultrasonication-three roll milling process will be used to processing the GNP/epoxy mixture.

Moreover, a further understanding of electromechanical properties by analytical modelling is carried out. In this regard, there are many studies trying to model the electrical properties of GNP based nanocomposites [24-27]. However, most of these studies do not provide a proper overview of electromechanical properties as do not take some parameters such as dispersion state or carbon nanoparticle interactions into account. Furthermore, the electrical behavior under compressive loads is not yet well understood as some studies have reported an increase of electrical resistance at compressive strain that, at first sight, is not easy to explain [28,29].

For these reasons, tensile and compressive tests will be carried out in the developed GNP strain sensors. The idea is to further explore the main mechanisms governing the electromechanical behavior of the proposed materials. In this regard, compressive behavior will be deeply analyzed by an analytical modelling which takes Poisson effect into account. This model is based in a previously one developed for bulk nanocomposites and proved at tensile load conditions [21]. Here, the interactions between nanoparticles have a crucial effect in electrical properties, in a similar way than for CNT based nanocomposites [30] and the effect of dispersion and GNP distribution inside the matrix will be deeply explored to better understanding the previously commented anomalous behavior at compressive load.

Furthermore, the reversibility of the proposed strain sensors will be also investigated by an analysis at different maximum load levels and at tensile and compressive stresses. It would highlight the potential and applicability of the GNP nanocomposite based strain sensors.

2. Materials and methods

2.1. Materials

The epoxy matrix of the surface sensors was bisphenol A diglycidyl ether (DGEBA) monomer (*Araldite LY556, Huntsman*) cured with an aromatic amine (*Araldite XB3473, Huntsman*). Graphene nanoplatelets were grade *M25* from *XGScience*, with an average lateral size of 25 µm and a thickness lower than 6 nm. They were used as nanoreinforcement to achieve electrically conductive nanocomposites. The GNPs content used was 3 wt%, based on a previous published work [3], which is near the percolation threshold to maximize the electrical sensitivity to strain.

2.2. Manufacturing of GNP/epoxy surface sensors

Dispersion of the GNPs into the epoxy matrix was carried out following a sonication and calandering two-step method. Initially, GNPs were incorporated into the DGEBA monomer and dispersed by probe sonication (*Hielscher UP400S*) with an amplitude of 50 % and a cycle of 0.5 s for 45 minutes. After sonication was completed, three cycles of three roll milling, using a mini-calander (*Exakt 80E, Exakt GmbH*), were applied with a gap distance between rolls of 5 µm and an increasing speed of 250, 300 and 350 rpm. A deeper analysis of the morphology of the nanocomposites and GNPs structure changes induced by the dispersion process have been published in a previous work proving the combined exfoliating and stretching effect of both dispersion procedures [31]. Once dispersion was done, the mixture was degassed under vacuum for 15 minutes and hardener was added. This degasification step is carried out before the hardener addition due to the low gel time of the mixture.

When the mixture was homogeneous, surface sensors were prepared by using a polytetrafluoroethylene (PTFE) mask on the surface of a glass reinforced composite substrate to produce a sensor with dimensions 50 x 5 mm. Dimensions of the substrates were 100 x 12 x 3 mm. Curing cycle was set at 140 °C for 8 hours and then, the polymeric mask was removed.

2.3. Electromechanical and microstructural characterization

The electromechanical performance of the GNP/epoxy strain sensors was analyzed under different load conditions. Mechanical tests were carried out in a *Zwick/Roell Z100 kN* machine following the correspondent ASTM standard for tensile (ASTM D 3039/D3039M – 00), compression (ASTM D3410) and flexural (ASTM D790 – 02) tests of polymer matrix reinforced composites. Test rate at both tensile and compression tests were fixed at 5 mm/min and 1.23 mm/min for flexural ones. Additionally, the maximum strain set in tests was below the value of the strain at break and yield strength, based on a previous published work [32]. Tensile elastic modulus, strength and elongation at break were 2.54 ± 0.07 GPa, 55.7 ± 3.7 MPa and 0.030 ± 0.004, respectively. Flexural elastic modulus, strength and elongation at break were 2.5 ± 0.4 GPa, 83.6 ± 7.9 MPa and 0.028 ± 0.004, respectively.

The electrical response of the strain sensors was simultaneously recorded by using a source-meter *Agilent 34410A*. In order to measure the electrical resistance, two copper electrodes were attached to the surface of the strain sensors with silver paint to minimize the electrical contact resistance. To avoid detachment during the tests, the electrodes were fixed with hot melt adhesive. Electrical sensitivity was determined as the change of the normalized resistance, $\Delta R/R_O$ divided by the applied strain, ε at different strain levels.

Thickness of strain sensors has been determined by using an optical profilometer *ZETA Z-20* and the microstructure of transversal section has been analyzed by Scanning Electron Microscopy (SEM) with a *S-3400N* apparatus from *Hitachi*. Samples were coated by sputtering with a thin layer of gold for a proper observation.

3. Results and discussion

3.1. Electromechanical characterization of GNP/epoxy strain sensors

The in-plane dimensions of the GNP/epoxy strain sensors, as it has been previously indicated, were 50 × 5 mm. Figure 1 shows the optical profilometry of the strain sensors, being the thickness ~ 300 μm. Furthermore, Figure 2 shows a representative SEM image of transversal section of strain sensors. Here, a good homogeneity of GNP distribution is observed due to the combined effect of ultrasonication, which induces partial exfoliation of GNP layers and three roll milling, which induces as stretching effect on thinner GNP particles due to the shear forces involved during dispersion [33].

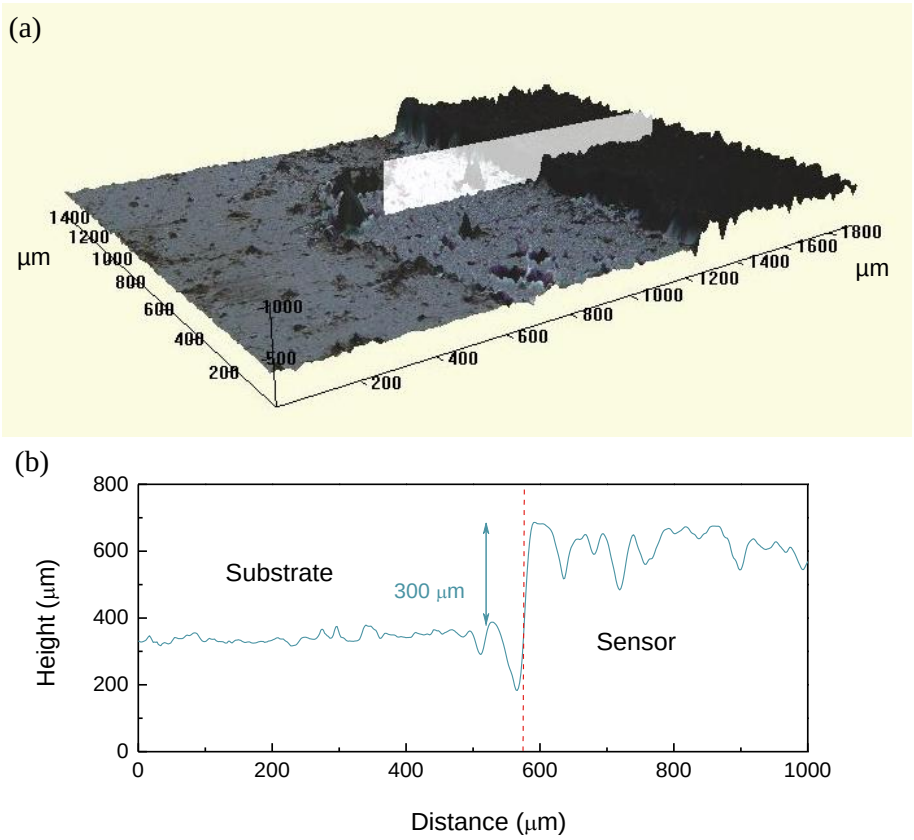

Figure 1. Analysis of thickness of surface sensors by optical profilometry: (a) 3D profile and (b) cross-sectional profile.

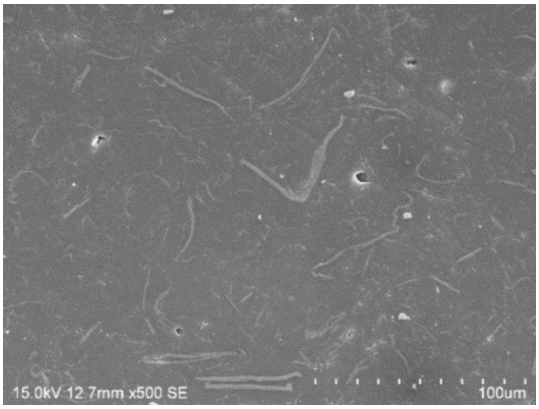

Figure 2. SEM image of the cross-section of GNP/epoxy surface sensors showing the distribution of GNPs within the cured nanocomposite.

3.1.1 Experimental analysis of sensitivity at tensile/compression

Figures 3a and 3b show the electromechanical response of the GNP/epoxy strain sensors under uniaxial tensile loads up to two different levels of maximum load, 2500 and 4000 N, in order to avoid failure of sensors. Two different maximum loads are used with the aim of analyzing possible changes in tendencies related to the strain level reached in the material, as opening of microcavities or internal defects, which can condition the electromechanical behavior and recovery of sensors. It can be seen that the normalized electrical resistance experiences an exponential growth as the one observed in volumetric sensors, behavior that has been previously published [34], which corresponds to a higher contribution of the tunneling conductivity along the GNPs paths. When load ceases, the strain sensors fully recover the initial state, demonstrating the reversibility of the created electrically conductive network. The sensitivity obtained was 9.1 ± 0.9 and 11 ± 1 for strain values up to 0.005 mm/mm and above 0.015 mm/mm, respectively. These values are lower to that obtained in the equivalent volumetric sensor, reinforced with the same GNPs content. The observed reduction is ~30 % for low strain values and ~60 % in the case of higher strain. This fact also evidences the higher linearity of the electrical response, as there is no significant difference between sensitivity values at low and high strain levels, which is indicative of a higher contribution of the electrical contact-based mechanisms. The increase in the contribution of this mechanism could be attributed to a slight preferential orientation of the GNPs

along the in-plane direction (Figure 2) or the volume analyzed, which is smaller than the one analyzed in volumetric samples [24]. This slight preferential orientation contributes to the creation of a more efficient 2D - electrical network, which results in higher concentration of electrical contacts of overlying GNPs and, consequently, in a higher linearity of the electrical response while the sensor is strained.

The electrical response of the GNP/epoxy strain sensors under compressive load was also studied. Representative results up to two different levels of maximum loads, 2000 and 6000 N, are shown in Figures 3c and 3d, respectively. Three different regions can be differentiated, similar to the ones obtained in volumetric sensors and the electrical response previously published by Han et al. [35] for similar systems. Initially, there is a diminution of the normalized electrical resistance (I), which appears at the two levels of maximum load, associated to the approximation of the adjacent GNPs, as well as an increase of contact area related to overlaying GNPs; followed by stabilization (II) and a consecutive increase (III), associated to separation of the GNPs and the partial interruption of electrically conductive paths, only observed in Figure 3d. As a consequence, calculated sensitivity under compressive loads was negative at low strain values (region I), being -13 ± 2; and positive at high strain (region III), with a value of 8 ± 1. The strain associated to the change in tendency is located at 0.018 mm/mm. Comparing these values to the ones of the volumetric sensors, the sensitivity is higher in both strain ranges [34]. Although the reasons are not clear, differences can be attributed to the volume contributing to the electrical measurement, which is lower in these strain sensors as mentioned above. However, although similar results under compressive load has been previously reported, as commented, it is necessary a deeper understanding of the electromechanical behavior of the proposed sensors subjected to this type of load.

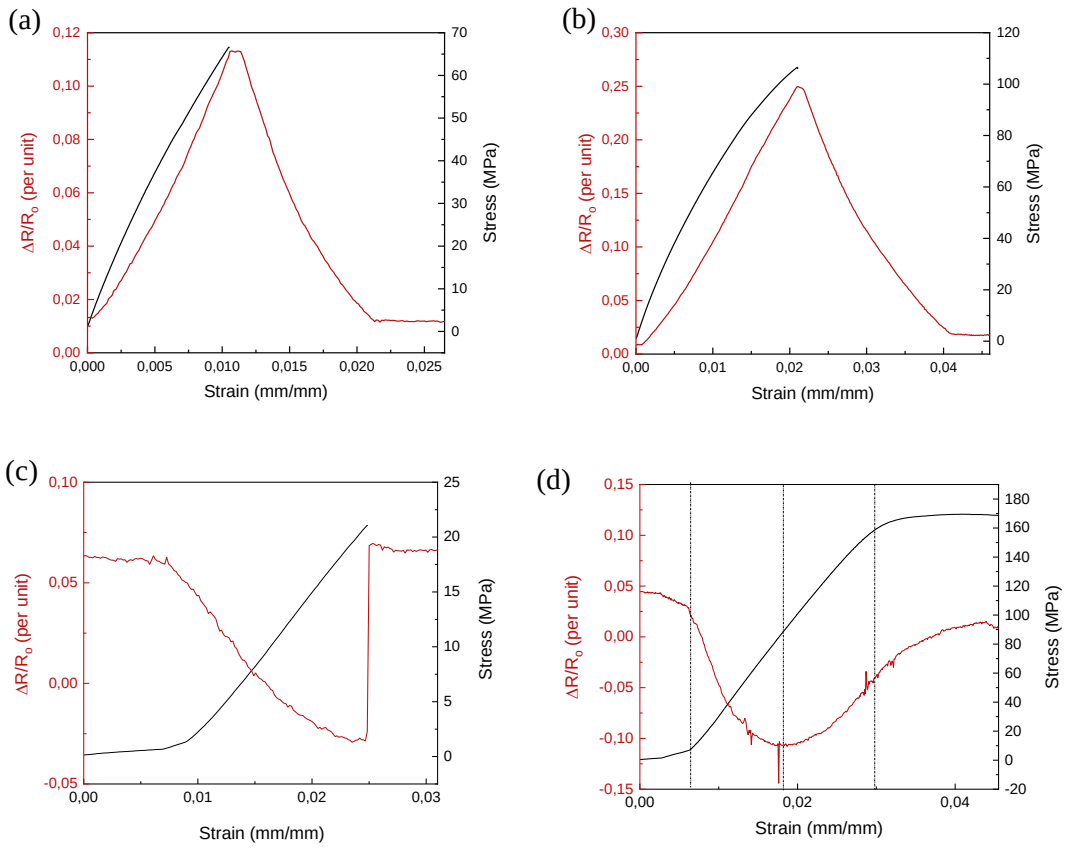

Figure 3. Electromechanical response of GNP/epoxy surface sensors under uniaxial load: (a, b) tensile up to (a) 2500 and (b) 4000 N, and (c, d) compression up to (c) 2000 and (d) 6000 N.

3.1.2 Theoretical analysis of electromechanical behavior

The analysis of the electromechanical properties, based on a theoretical model previously published [21], is carried out to better understanding the electrical properties of developed surface strain sensors.

This theoretical model is based on two types of tunneling mechanisms: out-of-plane (or type I) and in-plane (or type II). The electrical resistance variation is estimated by following the well-known exponential formula [36,37] as a function of tunneling distance:

$$R_T = (1-f)R_I + fR_{II}$$

$$R_I = \frac{h^2 t_I}{A_I e^2 \sqrt{2m\varphi}} exp\left(\frac{4\pi t_I}{h}\sqrt{2m\varphi}\right) \quad (1)$$

$$R_{II} = \frac{h^2 t_{II}}{A_{II} e^2 \sqrt{2m\varphi}} exp\left(\frac{4\pi t_{II}}{h}\sqrt{2m\varphi}\right)$$

Where *f* is the fraction of in plane contacts, *A* is the tunneling cross-sectional area, *e* and *m* are the electron charge and mass, respectively; *h* is the Planck's constant, φ is the height barrier of the epoxy and t_I and t_{II} are the tunneling distances of type I and type II contacts respectively, that can be calculated attending the following expression:

$$t_I = (1-\nu\varepsilon)t_{IO}^M$$

$$t_{II} = (1+\varepsilon)t_{IIO}^M \quad (2)$$

Here, it can be noticed that, for compressive loading, there is an increase on type I tunneling distance due to Poisson effect. This increase could lead to an overall increase of electrical resistance explained by a prevalence of out-of-plane contacts. Figure 4a summarizes the effect of *f* parameter on the electrical resistance variation for a given in-plane and out-of-plane contact areas. It can be observed that the electromechanical behavior of GNP nanocomposites is significantly different depending on the prevalence of contacts inside the electrical network. More specifically, the higher the value of *f* parameter, the higher the decrease of the electrical resistance due to the prevalence of type II contacts. However, at lower values of *f* parameter, it is possible to see an initial decrease of electrical resistance and, after that, an increase. This is explained by a prevalence of type II contacts at lower strain levels and a prevalence of type I contacts at higher strain levels, in a similar way than previously observed for tensile testing in nanocomposites [21].

In this context, Figure 4b shows the effect of the in-plane and out-of-plane tunneling areas on electromechanical response of strain sensors under compressive loading. It is observed that, the higher the correlation between type I and type II areas, the higher the prevalence of type II

tunneling mechanisms on electromechanical response, as type I area is more prevalent leading, thus, to a reduction of R_I, which promotes a lower contribution of this type of contact to the total electrical resistance.

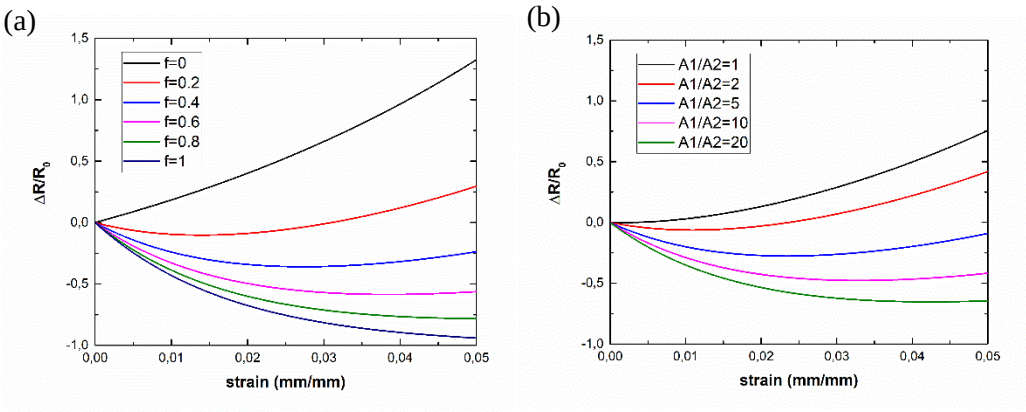

Figure 4. Influence of (a) *f* parameter and (b) correlation between Ai/Aii on electromechanical response of strain sensors.

Therefore, by knowing the effect of geometrical interactions between GNPs on electromechanical response, it is possible to adjust the theoretical model to experimental measurements under compressive loading. In this regard, Figure 5 shows the comparison of theoretical predictions to experimental results. A good agreement is observed between analytical predictions and empirical measurements. Here, the value of parameters *f* is fitted at 0.22, being similar to other studies where a *f* value at the same content was fitted at 0.19. The slight differences between *f* values are explained by a higher 2D disposition of nanoparticles in the strain sensors, leading to a slightly higher prevalence of type II electrical contacts.

As a conclusion, a better understanding of electrical response under compressive conditions is achieved, a fact that remained to be investigated.

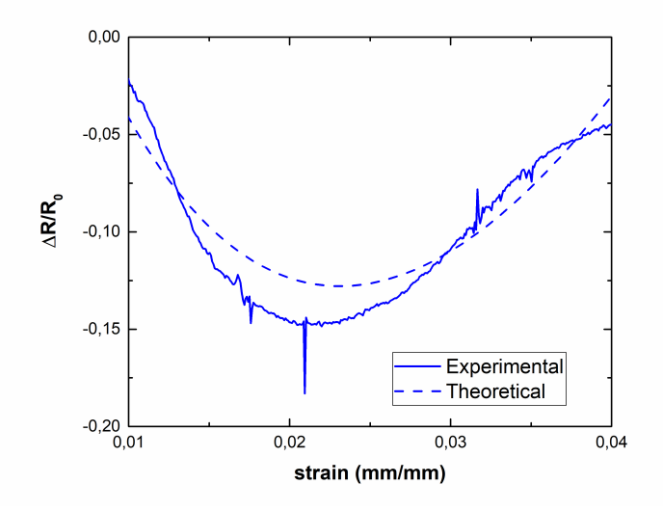

Figure 5. Experimental to theoretical response at compressive loading (dashed line indicates the electrical response of the fitted analytical model).

3.1.3 Analysis of sensitivity under flexural loading

Under flexural loads (Figure 6), two strain sensors were placed on the substrate surface, one on the tensile-subjected surface and the other on the compression-subjected one. When the surface subjected to tensile load was monitored (Figure 6a), an exponential tendency was observed, with a sensitivity of 160 ± 2 for applied loads between 0.003-0.006 mm/mm. This means an order of magnitude superior to that of the equivalent uniaxial load. Additionally, the electrical behavior of the sensor located onto the compression subjected surface (Figure 6b) showed a similar behavior to the one of the uniaxial compression load, but also with higher sensitivity, being -26 ± 4 and 44 ± 4 in zones I and III, respectively. The strain associated to the change in tendency, in this case, is located at $4.5 \cdot 10^{-3}$ mm/mm, which corresponds to a lower strain value compared to the one obtained under uniaxial compression loading. The increase of the sensitivity and the displacement to lower strain values of the strain threshold, i.e. transition between regions I and III, can be attributed to the bending of the sensor.

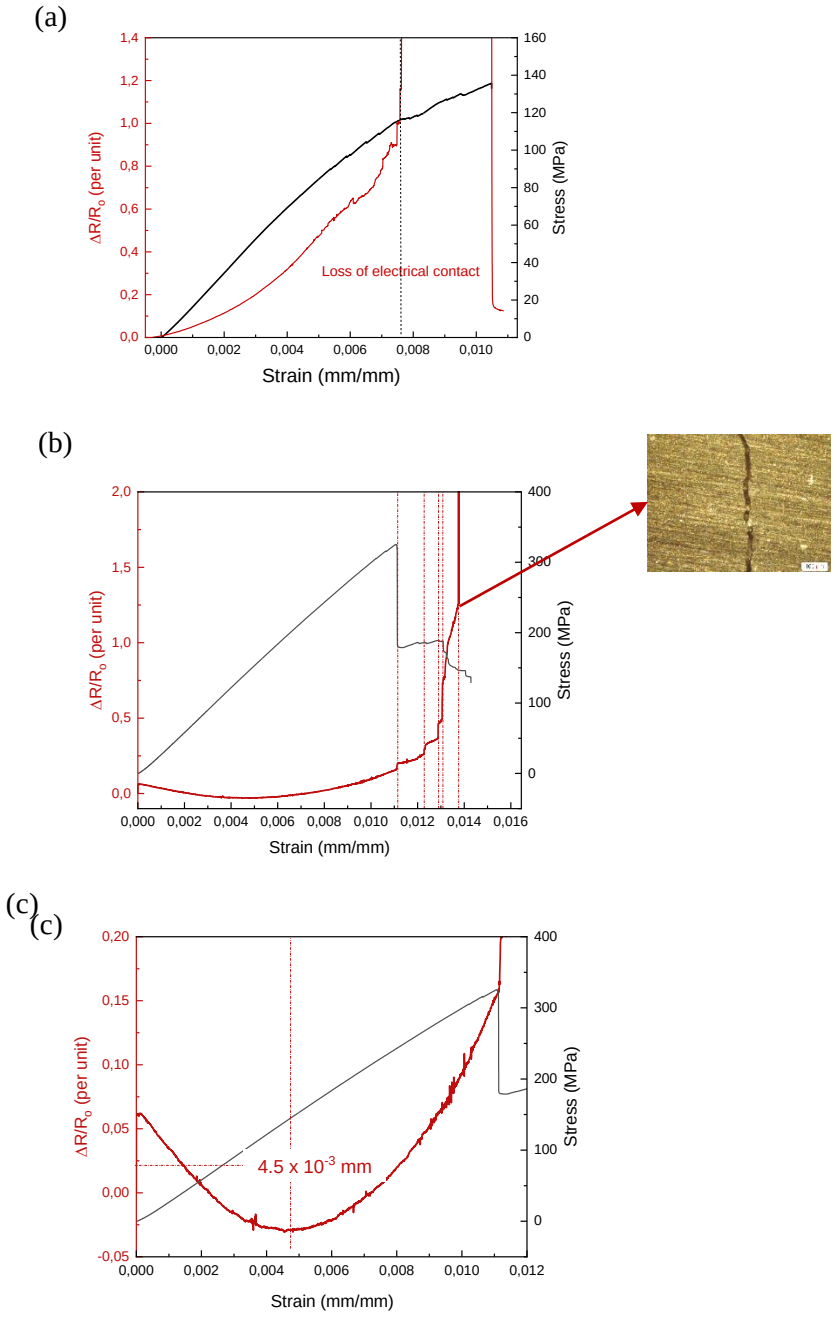

Figure 6. Electromechanical response of GNP/epoxy surface sensors under flexural load located onto: (a) tensile and (b) and (c) compressive subjected face where (c) is a magnification of the detailed electromechanical response of (b).

3.2. Reversibility under cyclic loading of GNP/epoxy strain sensors

Once the electrical response and sensitivity of the GNP/epoxy strain sensors have been analyzed, reversibility under cyclic loading needs to be assessed. Representative results of the electromechanical response of the strain sensors during 5 cycles under cyclic uniaxial tensile load are shown in Figure 7. It can be seen that reversibility of the sensors is complete, the initial state of the electrical network created by the GNPs is completely achieved and the amplitude of the normalized electrical resistance is constant along the cycles, as it has been observed by H. Hosseini et al [38], S. P. Patole et al. [39] and S. H. Min et al. [40] in similar sensors previously published.

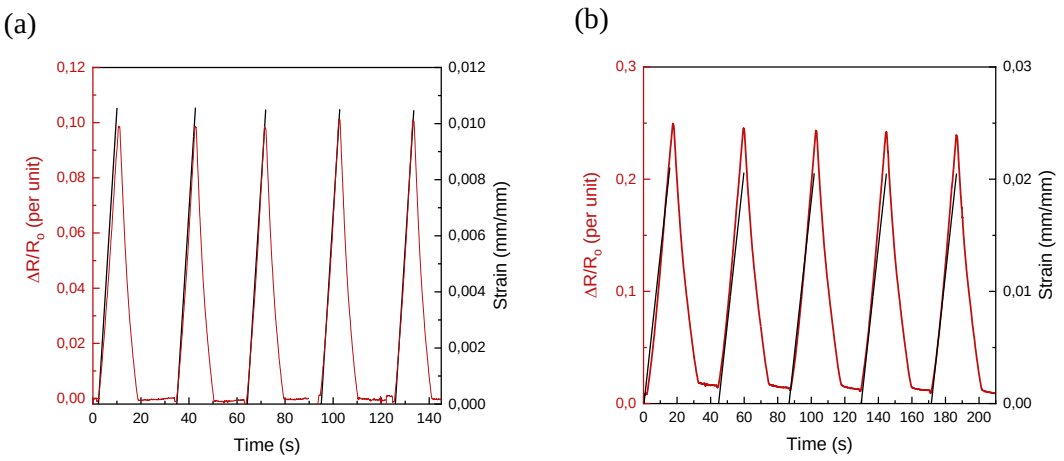

Figure 7. Electromechanical response of GNP/epoxy surface sensors under tensile cyclic load up to a maximum load of: (a) 2500 and (b) 4000 N.

In contrast, the electrical performance of the strain sensors under cyclic uniaxial compression load differs. Figure 8 shows the electromechanical behavior for four maximum loads: 2500 (Figure 8a), 4000 (Figure 8b), 5000 (Figure 8c) and 6000 N (Figure 8d). If the cyclic electrical response up to 2500 N is analyzed, which lies in region I, it can be noticed that reversibility of the sensors is fully achieved, although a slight increment in the amplitude of the signal can be appreciated. This could be attributed to the closing of internal defects. For higher loads, which induce strains

above 0.018 mm/mm, i.e. reaching region III, hysteresis in the electrical response was observed (Figures 8b-8d). The normalized electrical resistance does not follow the same path during loading and unloading, resulting in an asymmetric electrical response. The asymmetry of the curves is more significant as the maximum load reached during the test increases and, consequently, the maximum strain induced in strain sensors.

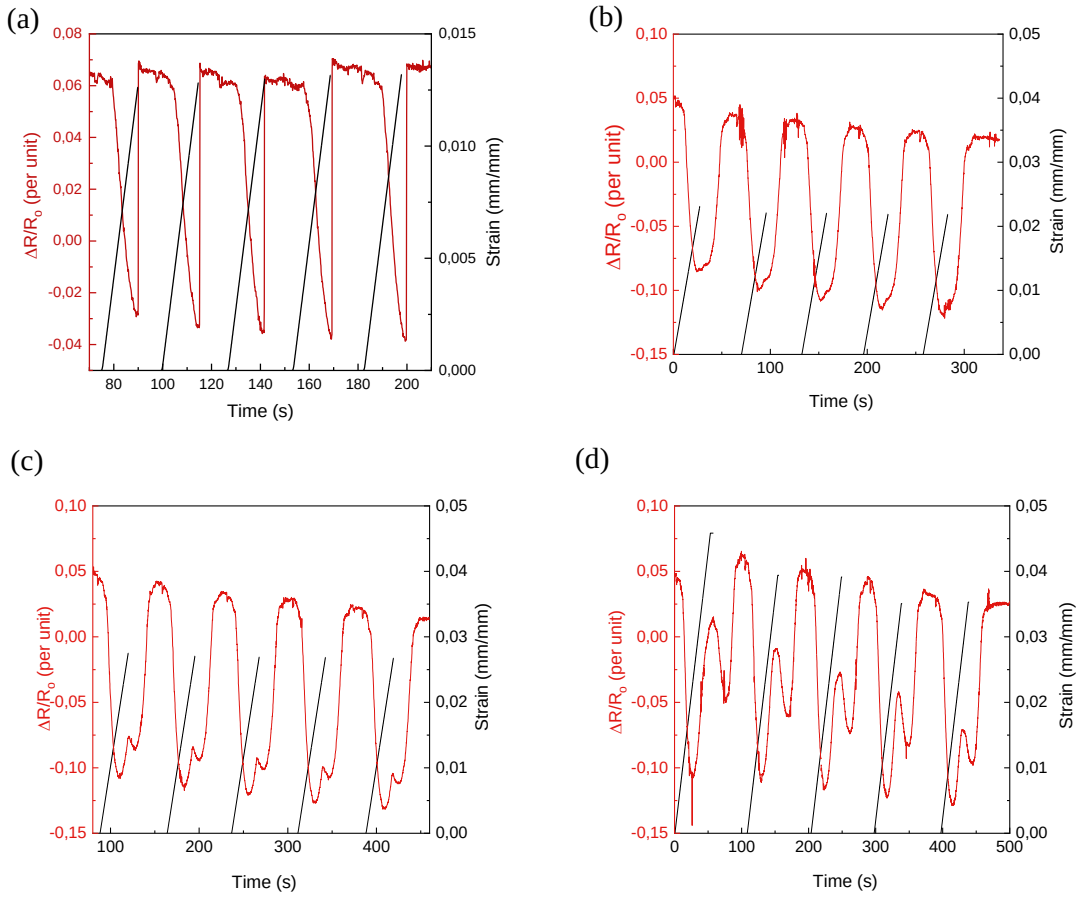

Figure 8. Electromechanical response of GNP/epoxy surface sensors under compressive cyclic load up to a maximum load of: (a) 2500, (b) 4000 N, (c) 5000 and (d) 6000 N.

With the aim of deeper studying the asymmetry mentioned above, calculated sensitivity (in regions I and III) and amplitude of the electrical response during loading and unloading are included in Table 1. From these values, a lower sensitivity during unloading is detected.

At strain values lower than 0.018 mm/mm, the reduction of sensitivity during unloading, related to the loading values, increases with the maximum applied load, being a diminution of 18, 21 and 27 % for 4000, 5000 and 6000 N, respectively. Additionally, there is also a decrease in the amplitude of the electrical signal, showing decays of 9, 17 and 29 %, respectively. Although the electrical performance varies depending on the maximum strain, i.e. sensitivity and amplitude of the electrical signal, these values remains the same for the different cycles at a same maximum load. This fact is important to be pointed out as it demonstrates reproducibility of the results. It can be affirmed that developed GNP/epoxy strain sensors present, in a certain way, reversibility if the whole cycle is treated like a module as it is repetitive with cycles.

Table 1. Electrical parameters during compressive cyclic loading and unloading.

Max. Load	**Cycle**	**Sensitivity $\varepsilon < 0.018$ mm/mm**		**Signal amplitude $\Delta R/R_o$**		**Sensitivity $\varepsilon > 0.018$ mm/mm**	
		Loading	**Unloading**	**Loading**	**Unloading**	**Loading**	**Unloading**
4000	1	-19 ± 2	16 ± 1	0.132 ± 0.004	0.127 ± 0.005	-	-
5000	1	-18 ± 2	14 ± 2	0.154 ± 0.001	0.128 ± 0.002	5.6 ± 0.6	-1.6 ± 0.3
6000	1	-17 ± 2	13 ± 2	0.164 ± 0.008	0.116 ± 0.005	7 ± 2	-5.4 ± 0.9

The reduction of the amplitude of the electrical signal with cycles, and the absence of changes after successive cycles with a same maximum strain, can be explained by the opening of micro-cavities in the vicinities of the GNPs, which has been previously corroborated in a published work [29]. The authors previously cited, Han et al. [35], also supported this statement in their published work. They propose that compressive forces induces the reduction of internal defects, such as holes, fissures, etc. This phenomenon leads to a reversible electrical response below a stress threshold, which authors suggest to be located at a 30% of the materials strength and is in accordance with the obtained behavior. Other authors, as Zhai et al. [41], have also published asymmetrical electrical responses in similar systems. Based on these discussions, at

first stages, due to the compressive stress, internal defects are closed as well as GNPs approximate each other, contributing to a diminution of the electrical. Once the stress is high enough, micro-cavities can be more prevalent, leading to an increase of the normalized electrical resistance of the strain sensors. These defects cannot be recovered during unloading but they can be closed during the initial stage of the next cycle. This fact justifies the increase of the amplitude and the negative slope of the base line. In this regard, Figure 9 shows a simplified model of mechanisms that occurs during deformation under tensile and compressive loads.

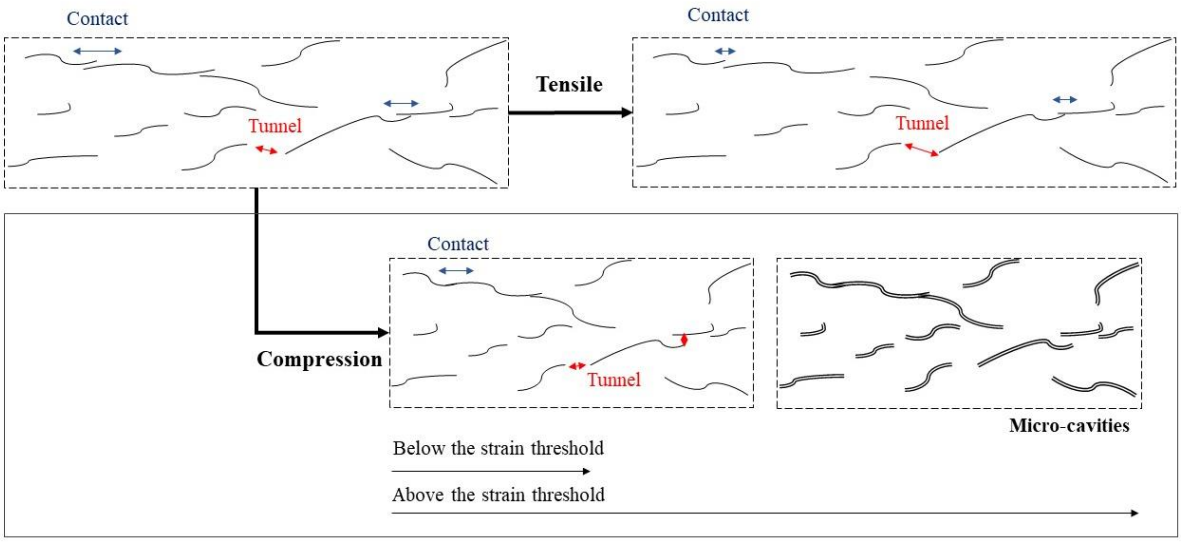

Figure 9. Simplified model of modifications induced in the electrical network created by the GNPs under tensile and compressive loads showing more significant mechanisms.

4. Conclusions

An experimental to theoretical study of strain monitoring mechanisms of GNP/epoxy strain sensors is carried out,

It is observed that the sensitivity at tensile loading is lower than the one of volumetric sensors from other studies. More specifically, measured GF was 9.1 ± 0.9 and 11 ± 1 for strain values up to 0.005 mm/mm and above 0.015 mm/mm, respectively This fact is associated to a higher linearity based on a prevalence of contact conducting mechanisms. Additionally,

electromechanical behavior when subjected to compressive strain is quite complex. An initial decrease is observed as expected due to a reduction in the tunneling distance between adjacent nanoparticles. Then, an increase of electrical resistance is noticed with calculated GF being negative at low strain values (region I), of -13 ± 2, and positive at high strain (region III), with a value of 8 ± 1. This is explained by the Poisson effect, leading to an increase of tunneling distance in transversal direction. By theoretical analysis, based on two types of contacts between GNPs: in-plane and out of plane, it can be elucidated that at lower strain level, there is prevalence of in-plane tunneling mechanisms whereas at higher strain levels the out of plane mechanisms dominate.

Tensile-compressive cyclic tests demonstrate the reversibility of the proposed strain sensors with similar baseline and peak resistance values. The slight differences during compressive cyclic tests can be attributed to the closing of internal defects during the cycle, leading to a different electrical response at load-unloading cycles.

Therefore, the proposed strain sensors show a good potential and applicability and a better understanding of electromechanical response under compressive conditions has been achieved.

Acknowledgements

The authors would like to thank the *Ministerio de Economía y Competitividad* of *Spain* Government (Project MAT2016-78825-C2-1-R) and Comunidad de Madrid Government (Project ADITIMAT-CM (S2018/NMT-4411)).

References

[1] Ruoff RS, Lorents DC. Mechanical and thermal properties of carbon nanotubes. carbon 1995;33(7):925-930.

[2] Yu MF, Lourie O, Dyer MJ, Moloni K, Kelly TF, Ruoff RS. Strength and breaking mechanism of multiwalled carbon nanotubes under tensile load. Science 2000;287(5453):637-640.

[3] Balandin AA, Ghosh S, Bao W, Calizo I, Teweldebrhan D, Miao F, Lau CN. Superior thermal conductivity of single-layer graphene. Nano letters 2008;8(3):902-907.

[4] Gomez-Navarro C, Burghard M, Kern K. Elastic properties of chemically derived single graphene sheets. Nano Letters 2008;8(7):2045-2049.

[5] Hamidinejad M, Zhao B, Zandieh A, Moghimian N, Filleter T, Park CB. Enhanced Electrical and Electromagnetic Interference Shielding Properties of Polymer-Graphene Nanoplatelet Composites Fabricated via Supercritical-Fluid Treatment and Physical Foaming. Acs Applied Materials & Interfaces 2018;10(36):30752-30761.

[6] Meng Q, Wu H, Zhao Z, Araby S, Lu S, Ma J. Free-standing, flexible, electrically conductive epoxy/graphene composite films. Composites Part A: Applied Science and Manufacturing 2017;92:42-50.

[7] Nistal A, Garcia E, Pérez -Coll D, Prieto C, Belmonte M, Osendi MI, Miranzo P. Low percolation threshold in highly conducting graphene nanoplatelets/glass composite coatings. Carbon 2018;139:556-563.

[8] Abbasi H, Antunes M, Ignacio Velasco J. Recent advances in carbon-based polymer nanocomposites for electromagnetic interference shielding. Progress in Materials Science 2019;103:319-373.

[9] Meng Q, Liu Z, Han S, Xu L, Araby S, Cai R, Zhao Y, Lu S, Liu T. A facile approach to fabricate highly sensitive, flexible strain sensor based on elastomeric/graphene platelet composite film. J Mater Sci 2019;54(15):10856-10870.

[10] Guadagno L, Raimondo M, Vittoria V, Vertuccio L, Naddeo C, Russo S, De Vivo B, Lamberti P, Spinelli G, Tucci V. Development of epoxy mixtures for application in aeronautics and aerospace. Rsc Advances 2014;4(30):15474-15488.

[11] Yang H, Yao X, Zheng Z, Gong L, Yuan L, Yuan Y, Liu Y. Highly sensitive and stretchable graphene-silicone rubber composites for strain sensing. Composites Science and Technology 2018;167:371-378.

[12] Datta S, Neerukatti RK, Chattopadhyay A. Buckypaper embedded self-sensing composite for real-time fatigue damage diagnosis and prognosis. Carbon 2018;139:353-360.

[13] Tallman T, Gungor S, Wang K, Bakis C. Damage detection and conductivity evolution in carbon nanofiber epoxy via electrical impedance tomography. Smart Mater Struct 2014;23(4):045034.

[14] García-Macías E, Rodríguez-Tembleque L, Saez A, Ubertini F. Crack detection and localization in RC beams through smart MWCNT/epoxy strip-like strain sensors. Smart Mater Struct 2018.

[15] Patole SP, Reddy SK, Schiffer A, Askar K, Prusty BG, Kumar S. Piezoresistive and mechanical characteristics of graphene foam nanocomposites. ACS Applied Nano Materials 2019;2(3):1402-1411.

[16] Lu S, Chen D, Wang X, Shao J, Ma K, Zhang L, Araby S, Meng Q. Real-time cure behaviour monitoring of polymer composites using a highly flexible and sensitive CNT buckypaper sensor. Composites Science and Technology 2017;152:181-189.

[17] Sánchez-Romate XF, Moriche R, Jiménez-Suárez A, Sánchez M, Prolongo SG, Güemes A, Ureña A. Highly sensitive strain gauges with carbon nanotubes: From bulk nanocomposites to multifunctional coatings for damage sensing. Appl Surf Sci.

[18] Moriche R, Jiménez-Suárez A, Sánchez M, Prolongo SG, Ureña A. Sensitivity, influence of the strain rate and reversibility of GNPs based multiscale composite materials for high sensitive strain sensors. Composites Science and Technology 2018;155:100-107.

[19] Sánchez-Romate XF, Artigas J, Jiménez-Suárez A, Sánchez M, Güemes A, Ureña A. Critical parameters of carbon nanotube reinforced composites for structural health monitoring applications: Empirical results versus theoretical predictions. Composites Sci Technol 2019;171:44-53.

[20] Kuronuma Y, Takeda T, Shindo Y, Narita F, Wei Z. Electrical resistance-based strain sensing in carbon nanotube/polymer composites under tension: Analytical modeling and experiments. Composites Sci Technol 2012;72(14):1678-1682.

[21] Sánchez M, Moriche R, Sánchez-Romate XF, Prolongo SG, Rams J, Ureña A. Effect of graphene nanoplatelets thickness on strain sensitivity of nanocomposites: A deeper theoretical to experimental analysis. Composites Science and Technology 2019;181:107697.

[22] Han S, Chand A, Araby S, Cai R, Chen S, Kang H, Cheng R, Meng Q. Thermally and electrically conductive multifunctional sensor based on epoxy/graphene composite. Nanotechnology 2019;31(7):075702.

[23] Moriche R, Prolongo SG, Sánchez M, Jiménez-Suárez A, Sayagués MJ, Ureña A. Morphological changes on graphene nanoplatelets induced during dispersion into an epoxy resin by different methods. Composites Part B: Engineering 2015;72:199-205.

[24] Hicks J, Behnam A, Ural A. A computational study of tunneling-percolation electrical transport in graphene-based nanocomposites. Appl Phys Lett 2009;95(21):213103.

[25] Kim Y, Cha JY, Ham H, Huh H, So D, Kang I. Preparation of piezoresistive nano smart hybrid material based on graphene. Current Applied Physics 2011;11(1):S350-S352.

[26] Chiacchiarelli LM, Rallini M, Monti M, Puglia D, Kenny JM, Torre L. The role of irreversible and reversible phenomena in the piezoresistive behavior of graphene epoxy nanocomposites applied to structural health monitoring. Composites Sci Technol 2013;80:73-79.

[27] Wang W, Jayatissa AH. Computational and experimental study of electrical conductivity of graphene/poly(methyl methacrylate) nanocomposite using Monte Carlo method and percolation theory. Synth Met 2015;204:141-147.

[28] Wang L, Wang X, Li Y. Relation between repeated uniaxial compressive pressure and electrical resistance of carbon nanotube filled silicone rubber composite. Composites Part A: Applied Science and Manufacturing 2012;43(2):268-274.

[29] Moriche R, Jiménez-Suárez A, Sánchez M, Prolongo SG, Ureña A. Sensitivity, influence of the strain rate and reversibility of GNPs based multiscale composite materials for high sensitive strain sensors. Composites Science and Technology 2018;155:100-107.

[30] Kuronuma Y, Takeda T, Shindo Y, Narita F, Wei Z. Electrical resistance-based strain sensing in carbon nanotube/polymer composites under tension: Analytical modeling and experiments. Composites Sci Technol 2012;72(14):1678-1682.

[31] Moriche R, Prolongo SG, Sánchez M, Jiménez-Suárez A, Sayagués MJ, Ureña A. Morphological changes on graphene nanoplatelets induced during dispersion into an epoxy resin by different methods. Composites Part B: Engineering 2015;72:199-205.

[32] Prolongo S, Moriche R, Jiménez-Suárez A, Sánchez M, Ureña A. Advantages and disadvantages of the addition of graphene nanoplatelets to epoxy resins. European Polymer Journal 2014;61:206-214.

[33] Sanchez-Romate XF, Jimenez-Suarez A, Sanchez M, Guemes A, Urena A. Novel approach to percolation threshold on electrical conductivity of carbon nanotube reinforced nanocomposites. Rsc Advances 2016;6(49):43418-43428.

[34] Moriche R, Sanchez M, Jimenez-Suarez A, Prolongo SG, Urena A. Strain monitoring mechanisms of sensors based on the addition of graphene nanoplatelets into an epoxy matrix. Composites Sci Technol 2016;123:65-70.

[35] Han B, Ding S, Yu X. Intrinsic self-sensing concrete and structures: A review. Measurement 2015;59:110-128.

[36] Simmons JG. Generalized formula for the electric tunnel effect between similar electrodes separated by a thin insulating film. J Appl Phys 1963;34(6):1793-1803.

[37] Hu N, Karube Y, Yan C, Masuda Z, Fukunaga H. Tunneling effect in a polymer/carbon nanotube nanocomposite strain sensor. Acta Materialia 2008;56(13):2929-2936.

[38] Hosseini H, Kokabi M, Mousavi SM. BC/rGO conductive nanocomposite aerogel as a strain sensor. Polymer 2018;137:82-96.

[39] Patole SP, Reddy SK, Schiffer A, Askar K, Prusty BG, Kumar S. Piezoresistive and Mechanical Characteristics of Graphene Foam Nanocomposites. ACS Applied Nano Materials 2019;2(3):1402-1411.

[40] Min S, Lee G, Ahn S. Direct printing of highly sensitive, stretchable, and durable strain sensor based on silver nanoparticles/multi-walled carbon nanotubes composites. Composites Part B: Engineering 2019;161:395-401.

[41] Zhai T, Li D, Fei G, Xia H. Piezoresistive and compression resistance relaxation behavior of water blown carbon nanotube/polyurethane composite foam. Composites Part A: Applied Science and Manufacturing 2015;72:108-114.